Inorganic Chemistry
Article

Inorg. Chem. **2010**, *49*, 4491–4498 **4491**
DOI: 10.1021/ic902424z

Face-to-Face Dinuclear Scaffolds Composed of Tetraazamacrocyclic Charged and Neutral Complexes

Katarzyna Szczepaniak,[†] Urszula E. Wawrzyniak,[‡] Jarosław Kowalski,[§] Iwona Mames,[§] Renata Bilewicz,*[,‡] Przemysław Kalicki,[§] and Bohdan Korybut-Daszkiewicz*[,†,§]

[†]*Cardinal Stefan Wyszyński University, College of Science, Department of Mathematics and Natural Science, Dewajtis 5, 01-815 Warszawa, Poland,* [‡]*Department of Chemistry, Warsaw University, Pasteura 1, 02-093 Warszawa, Poland, and* [§]*Institute of Organic Chemistry, Polish Academy of Sciences, Kasprzaka 44/52, 01-224 Warszawa, Poland*

Received December 7, 2009

A new family of bismacrocyclic homo- and heteronuclear Ni and Cu complexes has been synthesized and characterized. The ligand scaffold is comprised of two 14-membered tetraazamacrocyclic sites held in cofacial orientation. The dinuclear complexes are unique in that one macrocyclic center is neutral while the other one is charged, although the ligand backbones are nearly identical. This leads to a binuclear system of two structurally similar components, differing in their electron-donor abilities. The crystallographically characterized structures in the solid state revealed similarity of the four dinuclear complexes studied. The metal−metal separations are between 4 and 5 Å. The strongest electrostatic intramolecular interactions occur in the molecules with neutral and charged components, most differing in donor abilities.

Introduction

The overall goal of using supramolecular dinuclear systems based on noncovalently[1−3] associated electroactive molecules, hydrogen bonds,[4] or coordinative metal bonds[5,6] is to achieve new organic materials. Bridged donor systems, either as supermolecules or assemblies on surfaces, have been carried out in order to construct molecular devices for application in electronics and photovoltaics.[7] They are also useful synthetic models for metalloproteins with more than one metal center.[8,9] Compounds containing separated metal units of similar structure in one molecule present simple models of multicenter catalysts and biological clusters found in enzymes. Such model systems enable investigation of the intramolecular interactions and specifically—evaluation of the effect of a similar redox unit located in the same molecule—of the redox properties of a given metallic center. They also enable one to pinpoint any nonlinearity of interactions in the multicenter system.

Investigations into porphyrin-based bridged donor systems, show how the intermetallic distances and the donor energy gaps affect the electronic coupling.[10] In the context of intramolecular interactions, ferrocene represented one of the first electron donors that was integrated, together with electron-accepting fullerenes, into a series of novel conjugates.[11] Over the past few years, the design of such multicomponent supramolecular systems containing covalently linked electroactive centers was continued and extended.

Bismacrocyclic complexes composed of two neutral[12] or two charged[8,9,13,14] tetraazamacrocyclic metal-complexing units were extensively studied. Host−guest interactions in

*Corresponding author. Telephone: +48 22 3432035. Fax +48 22 632 66 81. E-mail: bkd@icho.edu.pl.

(1) Wasielewski, M. R. *Chem. Rev.* **1992**, *92*, 435–461.
(2) Gayathri, S. S.; Wielopolski, M.; Pérez, E. M.; Fernández, G.; Sánchez, L.; Viruela, R.; Ortí, E.; Guldi, D. M.; Martín, N. *Angew. Chem., Int. Ed.* **2009**, *48*, 815–819.
(3) Chitta, R.; Sandanayaka, A. S. D.; Schumacher, A. L.; D'Souza, L.; Araki, Y.; Ito, O.; D'Souza, F. *J. Phys. Chem. C* **2007**, *111*, 6947–6955.
(4) Wessendorf, F.; Gnichwitz, J.- F.; Sarova, G. H.; Hager, K.; Hartnagel, U.; Guldi, D. M.; Hirsch, A. *J. Am. Chem. Soc.* **2007**, *129*, 16057–16071.
(5) Schumacher, A. L.; Sandanayaka, A. S. D.; Hill, J. P.; Ariga, K.; Karr, P. A.; Araki, Y.; Ito, O.; D'Souza, F. *Chem.−Eur. J.* **2007**, *13*, 4628–4635.
(6) D'Souza, F.; Gadde, S.; Schumacher, A. L.; Zandler, M. E.; Sandanayaka, A. S. D.; Araki, Y.; Ito, O. *J. Phys. Chem. C* **2007**, *111*, 11123–11130.
(7) Albinsson, B.; Martensson, J. *J. Photochem. Photobiol., C* **2008**, *9*, 138–155.
(8) Busch, D. H.; Christoph, G. G.; Zimmer, L. L.; Jackels, S. C.; Grzybowski, J.; Callahan, R. W.; Kojima, M.; Holter, K. A.; Mocak, J.; Herron, N.; Chavan, M. Y.; Schammel, W. P. *J. Am. Chem. Soc.* **1981**, *103*, 5107–5114.
(9) Hoshino, N.; Goldsby, K. A.; Busch, D. H. *Inorg. Chem.* **1986**, *25*, 3000–3006.
(10) Wiberg, J.; Guo, L.; Pettersson, K.; Nilsson, D.; Ljungdahl, T.; Martensson, J.; Albinsson, B. *J. Am. Chem. Soc.* **2007**, *129*, 155–163.
(11) Guldi, D. M.; Maggini, M.; Scorrano, G.; Prato, M. *J. Am. Chem. Soc.* **1997**, *119*, 974–980.
(12) Bilewicz, R.; Wieckowska, A.; Korybut-Daszkiewicz, B.; Olszewska, A.; Woźniak, K.; Feeder, N. *J. Phys. Chem. B* **2000**, *104*, 11430–11434.
(13) Domagała, S.; Wieckowska, A.; Kowalski, J.; Rogowska, A.; Szydłowska, J.; Korybut- Daszkiewicz, B.; Bilewicz, R.; Woźniak, K. *Chem.—Eur. J.* **2006**, *12*, 2967–2981.
(14) Wieckowska, A.; Bilewicz, R.; Domagała, S.; Woźniak, K.; Korybut-Daszkiewicz, B.; Tomkiewicz, A.; Mroziński, J. *Inorg. Chem.* **2003**, *42*, 5513–5522.

Published on Web 04/14/2010

Scheme 1

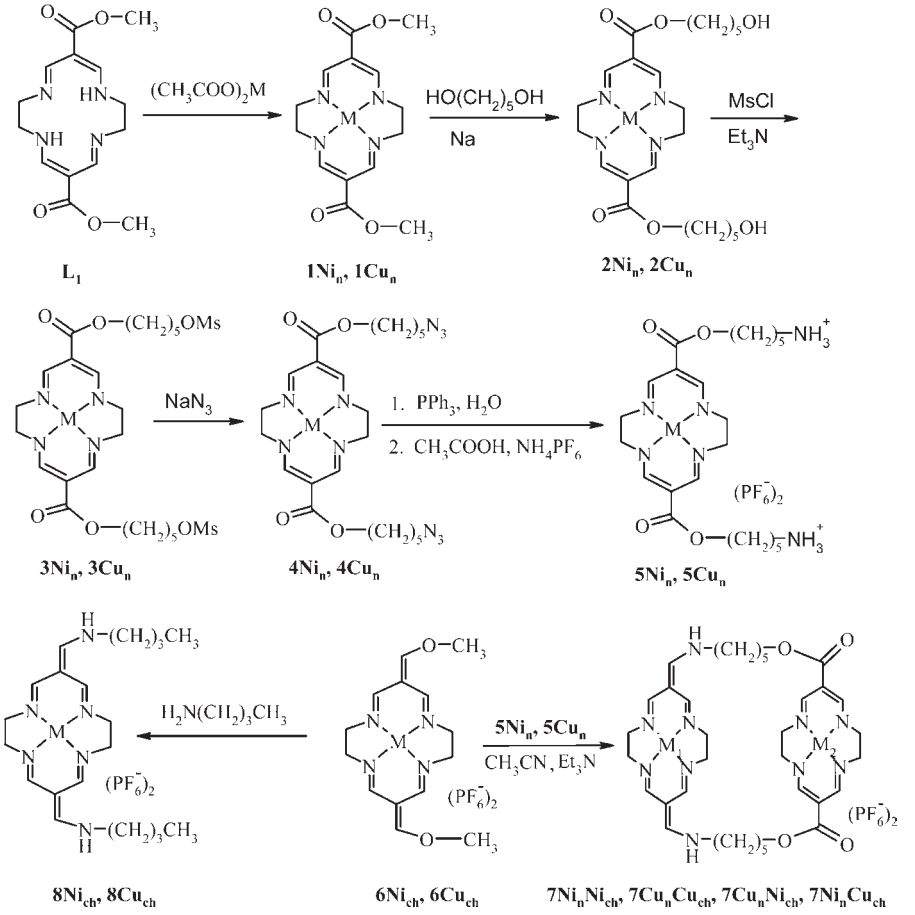

the gas phase between neutral complexes $\mathbf{1Cu_n}$ or $\mathbf{1Ni_n}$ (Scheme 1) and bismacrocyclic cations containing two charged cyclidene units linked with aliphatic chains were revealed by analyzing ESI mass spectra (ESI-MS).[15] Such interactions were also observed for neutral macrocyclic complexes ($\mathbf{1Cu_n}$ and $\mathbf{1Ni_n}$) attached through 3-mercaptopropyl chains to a gold electrode.[16,17] Therefore, the aim of this study was to design a series of model bismacrocyclic transition-metal complexes possessing one molecule, a charged and neutral donor macrocyclic unit separated by alkyl chains. Closed locations of electron-rich (neutral) and electron-deficient (charged) metal-complexing macrocycles in the same molecule give an opportunity to study mutual interactions between them.

The redox processes of this series of molecules are connected with the changes of oxidation states of the metallic centers and hence do not involve the production of radical species encountered in most of the purely organic systems. This in turn determines their stability, lack of interfering chemical reactions, and biocompatibility— all properties of utmost importance in future applications of the presented multicenter molecules. Their redox behavior can be tuned by changing the metal center cation, the length of alkyl bridges, and the structure of the macrocyclic ligand.

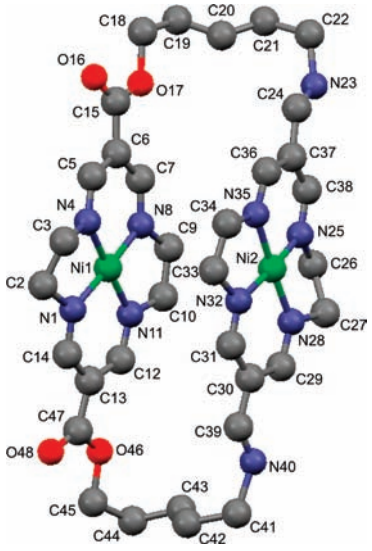

Figure 1. X-ray structure of $\mathbf{7Ni_nNi_{ch}}$ cation with the atom labeling scheme (hydrogen atoms, hexafluorophosphate anions, and water and solvent molecules were omitted for clarity). The labeling scheme is assigned analogously for all structures.

Results and Discussion

Synthesis. After standard transformations outlined in Scheme 1, the neutral dimethyl esters ($\mathbf{1Cu_n}$, $\mathbf{1Ni_n}$) gave

(15) Rybka, A.; Koliński, R.; Kowalski, J.; Szmigielski, R.; Domagała, S.; Woźniak, K.; Wieckowska, A.; Bilewicz, R.; Korybut-Daszkiewicz, B. *Eur. J. Inorg. Chem.* **2007**, 172–185.
(16) Wawrzyniak, U. E.; Woźny, M.; Kowalski, J.; Domagała, S.; Maicka, E.; Bilewicz, R.; Woźniak, K.; Korybut-Daszkiewicz, B. *Chem.—Eur. J.* **2009**, *15*, 149–157.
(17) Wawrzyniak, U. E.; Woźny, M.; Mames, I.; Pałys, B.; Korybut-Daszkiewicz, B.; Bilewicz, R. *Dalton Trans.* **2010**, *39*, 730–735.

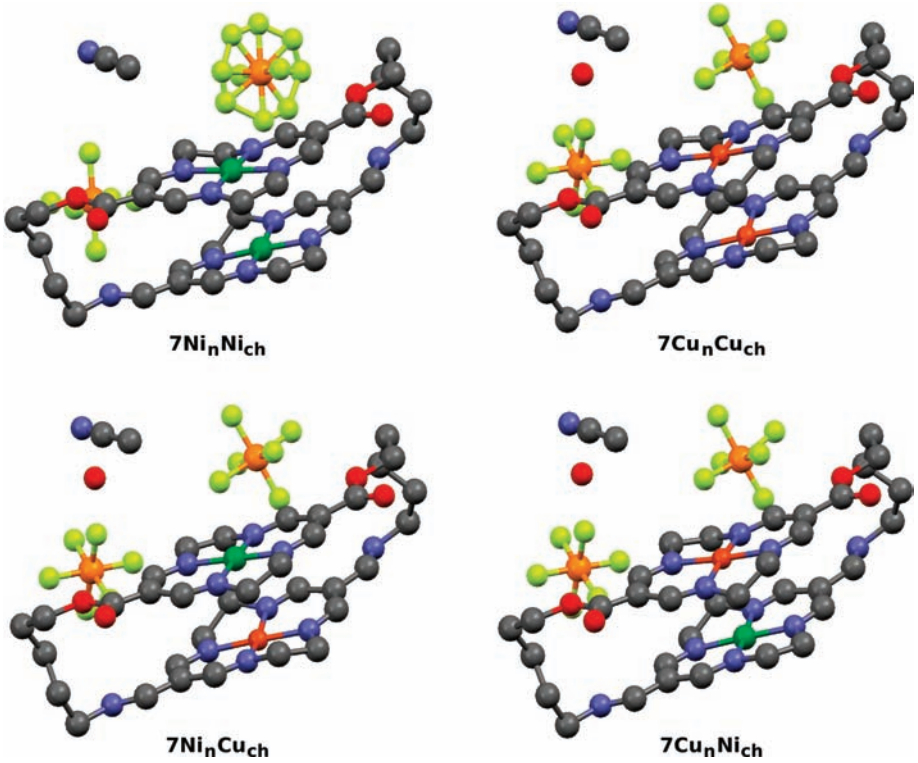

Figure 2. X-ray structures of all bismacrocyclic complexes.

complexes of protonated diamines **5Cu$_n$** and **5Ni$_n$**, which afterward were used as bridging units for the ring closure reaction around [14]cyclidenes **6Cu$_{ch}$** and **6Ni$_{ch}$**. All four possible combinations of dinuclear complexes coordinating nickel(II) and/or copper(II) in neutral and cationic macrocycles (**7Ni$_n$Ni$_{ch}$**, **7Ni$_n$Cu$_{ch}$**, **7Cu$_n$Ni$_{ch}$**, and **7Cu$_n$Cu$_{ch}$**) were synthesized and characterized. Reaction of **6Cu$_{ch}$** and 6Ni$_{ch}$ with *n*-buthylamine leads to the formation of linear products **8Cu$_{ch}$** or **8Ni$_{ch}$**. Structures of synthesized complexes were confirmed on the basis of elemental analyses and spectroscopic, mainly FD or ESI-MS and NMR, evidence.

Structural Details. All studied bismacrocyclic molecules form very similar crystals (Figure 1) and molecular structures crystallizing in the monoclinic $P2_1/n$ space group. Crystals were obtained as monohydrates also containing one acetonitrile molecule and two hexafluorophosphate anions (not interacting or interacting weakly with other atoms) per one bismacrocycle. There are four bismacrocyclic molecules in the unit cell, while only one is independent.

The geometry of compounds studied in this paper is similar to that of previously synthesized bis-[14]cyclidene complexes composed of two charged macrocyclic unites.[13,18] There are generally two opposite, nearly parallel, planar 14-membered tetraazamacrocyclic rings coordinating metal ions. Even visual inspection of the molecule **7** (see Figure 2) shows that their central cyclic fragments are attracting each other. The neutral moiety is slightly curved toward the inside of the macrocycle, while the cationic one bulges outward. The rings are also considerably shifted (ca. 2.5 Å)

(18) Wieckowska, A.; Bilewicz, R.; Domagała, S.; Woźniak, K.; Korybut-Daszkiewicz, B.; Tomkiewicz, A.; Mroziński, J. *Inorg. Chem.* **2003**, *42*, 5513–5522.

Table 1. Important Structural Parameters of Bismacrocyclic Complexes[a]

compound	7Ni$_n$Ni$_{ch}$	7Cu$_n$Cu$_{ch}$	7Ni$_n$Cu$_{ch}$	7Cu$_n$Ni$_{ch}$
mean M$_n$···N	1.838	1.916	1.858	1.908
mean M$_{ch}$···N	1.839	1.920	1.894	1.850
M$_n$···M$_{ch}$ intramol.	4.761	4.647	4.652	4.577
M′$_n$···M$_{ch}$ intermol.	4.498	4.504	4.535	4.606
C(20)···C(43)	13.332	13.471	13.483	13.442
mean C=C$_{exocyclic}$	1.404	1.422	1.405	1.408
mean =C−N$_{exocyclic}$	1.278	1.273	1.293	1.296
O48 ··· N23′	2.85	2.86	2.87	2.84
O1W···N40	−	2.92	2.93	2.89
O1W···F	−	2.96, 3.01	2.93, 3.00	2.96, 3.05

[a] Distances are in Å.

and a bit twisted (about 5°) to each other, and thus the conformations of polymethylene bridges are slightly different. The distances between central atoms of aliphatic linkers range from 13.432 to 13.483 Å. The shortest metal−metal distance (Table 1) was observed for **7Cu$_n$Ni$_{ch}$**. The molecules studied form three-dimensional (3D) lattices utilizing numerous weak intermolecular interactions. Bismacrocyclic cations are packed in such a way as to optimize interactions between the macrocyclic fragments from neighboring molecules. Thus, intermolecular metal−metal distances (Table 1) are even shorter in complexes **7Ni$_n$Ni$_{ch}$**, **7Cu$_n$Cu$_{ch}$**, and **7Ni$_n$Cu$_{ch}$** and only slightly longer in compound **7Cu$_n$Ni$_{ch}$** than the intramolecular ones. Coordination spheres of both macrocyclic units are square planar, and the metal−ligand distances are typical for copper(II) and nickel(II) complexes with 14-membered tetraimines. The lengths of the C−N bonds, linking the cationic units, are close to those usually observed for double bonds. On the other hand, the formally double, exocyclic C=C bond distances are close to typical for single bonds (Table 1). It is common in these kinds of complexes

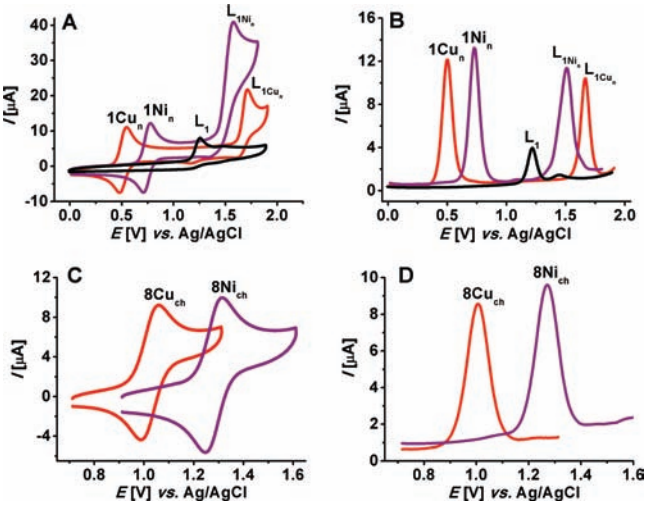

Figure 3. CV (A, C) and DPV (B, D) for 5×10^{-4} M (A, B) neutral $\mathbf{1Cu_n}$, $\mathbf{1Ni_n}$ and $\mathbf{L_1}$; (C, D) charged $\mathbf{8Cu_{ch}}$, $\mathbf{8Ni_{ch}}$ (ligand oxidation in the charged complexes is not accessible) in a 0.1 M TBAHPF/AN solution; (A, C) v = 0.05 V/s and (B, D) ΔE = 25 mV.

for the electron density of the exocyclic nitrogen atom to be conjugated with the delocalized electron density of the cationic macrocyclic ring, resulting in elongation of C=C and in shortening of C−N bond.

All structures show the presence of intermolecular hydrogen bonds. The strongest are formed between the exocyclic nitrogen atoms and the water molecule's oxygen as well as the carbonyl group. There are also some weaker hydrogen bonds between the water's oxygen and fluorine atoms.

Electrochemistry. We compare the redox properties of these new complexes with those of mononuclear neutral and charged complexes—the building blocks of the dinuclear molecules. Linear scan and differential pulse voltammetric techniques are employed to determine the changes of formal potentials of the redox centers, reflecting intramolecular interactions in the compounds. All of the macrocyclic complexes undergo close to reversible Me^{2+}/Me^{3+} electrode processes, and no other chemical reactions are involved. The comparison of formal potentials of the neutral monomacrocyclic complexes of Cu^{2+} and Ni^{2+} ($\mathbf{1Cu_n}$, $\mathbf{1Ni_n}$) and of the corresponding charged complexes ($\mathbf{8Cu_{ch}}$, $\mathbf{8Ni_{ch}}$) indicates that neutral complexes have stronger donor properties since their oxidation/reduction electrode processes appear at less positive potentials (Figure 3A and B and Table 2).

In the neutral copper complex, the electron density is more localized on the metallic center than in the nickel complex, which facilitates removal of the electron to the electrode—the oxidation peak appears at least positive potentials. On the other hand, the ligand oxidation peak in $\mathbf{1Cu_n}$ appears at the highest positive value in comparison with the free ligand ($\mathbf{L_1}$) and $\mathbf{1Ni_n}$, showing the relatively smaller charge density on the ligand. Hence, there is clear dependence of the potential of irreversible ligand oxidation (a_L) on the donor properties of the center. The same ligand in the nickel(II) complex is oxidized at a potential of 132 mV, less positive than that of the copper(II) compound (Figure 3A and B).

In the positively charged monomacrocyclic complex cations, the metal ion is surrounded by the azamacrocyclic ring accompanied by negatively charged counterions. The oxidation of Cu^{2+} and Ni^{2+} in the positively charged complexes occurs at more positive potentials than those of neutral ones. The order of formal potentials is same as in case of neutral complexes; Cu^{2+} is oxidized more easily to Cu^{3+} than Ni^{2+} is to Ni^{3+} (Figure 3C,D).

Table 2. Comparison of the Redox Properties of Monomacrocyclic Complexes and Homo- And Heterobismacrocyclic Complexes

compound	$E^{0'}M_n$[V]	$E^{0'}M_{ch}$ [V]	E_{pa}L[V]	ΔE[V] ($E^{0'}M_{ch} - E^{0'}M_n$)
$\mathbf{L_1}$	–	–	1.257	–
$\mathbf{1Ni_n}$	0.743	–	1.579	–
$\mathbf{8Ni_{ch}}$	–	1.280	–	–
$\mathbf{1Cu_n}$	0.511	–	1.711	–
$\mathbf{8Cu_{ch}}$	–	1.072	–	–
$\mathbf{7Ni_nNi_{ch}}$	0.767	–	1.587	–
$\mathbf{7Cu_nCu_{ch}}$	0.555	1.081	1.762	0.526
$\mathbf{7Cu_nNi_{ch}}$	0.542	1.396	1.708	0.854
$\mathbf{7Ni_nCu_{ch}}$	0.777	1.078	1.567	0.301

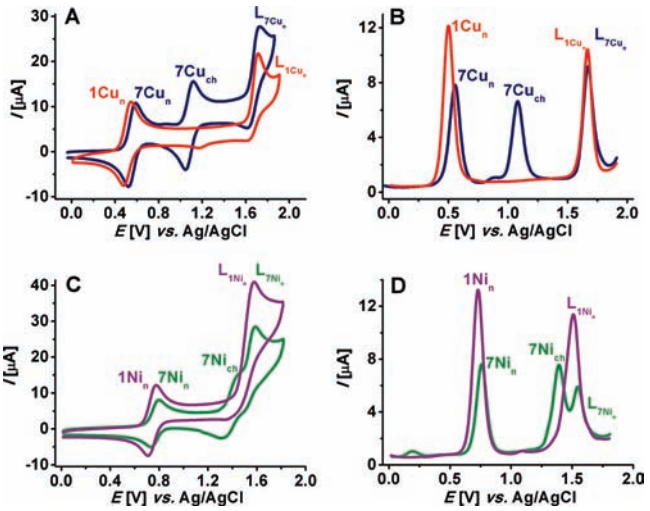

Figure 4. CV (A, C) and DPV (B, D) for 5×10^{-4} M (A, B) $\mathbf{1Cu_n}$ and $\mathbf{7Cu_nCu_{ch}}$; (C, D) $\mathbf{1Ni_n}$ and $\mathbf{7Ni_nNi_{ch}}$ in a 0.1 M TBAHPF/AN solution; (A) v = 0.05 V/s and (B) ΔE = 25 mV.

Transition-metal ions in monomacrocyclic the complexes of Cu^{2+} and Ni^{2+} oxidize easier than in the homodinuclear complexes of Cu^{2+} and Ni^{2+} ($\mathbf{7Cu_nCu_{ch}}$, $\mathbf{7Ni_nNi_{ch}}$) (Figure 4). In homonuclear bismacrocyclic copper complex $\mathbf{7Cu_nCu_{ch}}$, the redox potential of the neutral copper center is about 44 mV more positive than in the neutral mononuclear complex ($\mathbf{1Cu_n}$).

Nonlinearity Effects in Bismacrocyclic Complexes. The redox parameters and the diffusion coefficients of all the complexes studied in this work are collected in Tables 2 and 3. The presence of a charged macrocyclic complex in the bismacrocyclic molecule decreases the electron-donor abilities of the other center. This resembles the common behavior of a redox center in the presence of an electron-withdrawing substituent in the molecule—the donation of the electron to the electrode becomes more difficult. The donor neutral and charged components in the bismacrocyclic molecule interact with each other affecting their redox behavior compared to those of isolated metal centers. The separation between peak couples corresponding to each of the redox centers reflects stabilization of the mixed valence moiety. The most stable mixed valence state is that of $\mathbf{7Cu_nNi_{ch}}$. Interestingly, arranging

Table 3. Formal Redox Potentials and HOMO Values of Mono- And Bismacrocyclic Complexes

compound	$-E^{HOMO}M_{ch}$ (eV)	$-E^{HOMO}M_n$ (eV)	$E^{HOMO}M_{ch} - E^{HOMO}M_n$ (eV)
1Ni$_n$	–	5.118	–
8Ni$_{ch}$	5.655	–	–
1Cu$_n$	–	4.886	–
8Cu$_{ch}$	5.447	–	–
7Ni$_n$Ni$_{ch}$	–[a]	5.142	–
7Cu$_n$Cu$_{ch}$	5.456	4.930	0.526
7Cu$_n$Ni$_{ch}$	5.771	4.917	0.854
7Ni$_n$Cu$_{ch}$	5.453	5.152	0.301

[a] Peak overlapping with the ligand oxidation current.

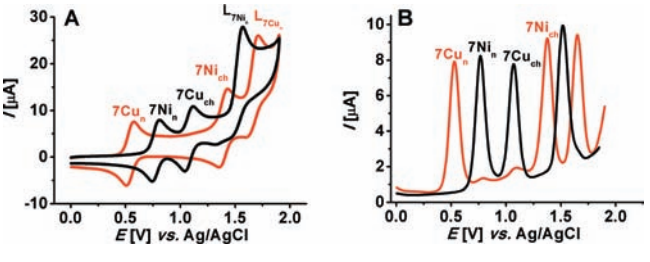

Figure 5. Comparison of CV (A) and DPV (B) for 5×10^{-4} M **7Cu$_n$Ni$_{ch}$**; **7Ni$_n$Cu$_{ch}$** in a 0.1 M TBAHPF/AN solution; (A) v = 0.05 V/s and (B) ΔE = 25 mV.

the centers in the opposite way (**7Ni$_n$Cu$_{ch}$**) leads to a significant decrease of the stability of the mixed valence form (Figure 5A and B).

The strongest stabilization of the mixed valence complex appearing in **7Cu$_n$Ni$_{ch}$** can be understood considering that, in this case, the more electron-rich unit (Cu^{2+} coordinated in the neutral tetraazamacrocyclic ring) is combined with the less electron rich one (Ni^{2+} in the charged tetraazamacrocycle).

For all bismacrocyclic complexes oxidation proceeds according to the E_1E_2 mechanism:[19]

$$M_1^{II}M_2^{II} - e \xrightarrow{E_1} M_1^{II}M_2^{III} - e \xrightarrow{E_2} M_1^{III}M_2^{III} \quad (1)$$

Additional equilibria are, therefore, those of reactions:

$$M_1^{II}M_2^{II} + M_1^{III}M_2^{III} \leftrightarrow 2M_1^{II}M_2^{III} \quad (2)$$

or/and

$$M_1^{II}M_2^{II} + M_1^{III}M_2^{III} \leftrightarrow 2M_1^{III}M_2^{II} \quad (3)$$

The reaction 3 constant (K), reflecting the stability of the mixed valent state of the complex, was evaluated based on the equation:

$$K = \exp\left[\frac{\Delta E \cdot F}{RT}\right] \quad (4)$$

where, ΔE [V] is the difference in the formal potentials for the 1e processes at two metal centers (identical or nonidentical); F stands for the Faraday constant, 96 500 C; R is the gas constant; 8.31 J mol^{-1} K^{-1}; and T is temperature (298 K).

(19) Zanello, P. *Inorganic Electrochemistry. Theory, Practice and Application*, Royal Society of Chemistry: Cambridge, 2003; p 174.

At 298 K,

$$K = 10^{16.9\Delta E} \quad (5)$$

Large K values of the bismacrocyclic compounds studied reflect high stability of the mixed valence state (Table 2).

The highest occupied molecular orbital (HOMO) energy values for mono- and bismacrocyclic complexes were determined from the formal potential values of the metal center with respect to ferrocene (Fc), as shown in Table 3. All data were calculated based on the reference energy level of Fc (4.8 eV below the vacuum level) according to $E^{HOMO} = -[4.8 + (E^{0'} - E^{0'}Fc)]$.[20,21] Neutral monomacrocyclic complex of Cu^{2+} (**1Cu$_n$**) has the highest HOMO energy value of −4.886 eV, and accordingly, it is expected to have the lowest barrier to hole injection from the electrode surface.

The energy levels of monomacrocyclic complexes are different from those in the bismacrocyclic compounds (Table 3).

We calculate the difference in energy levels of the components in bismacrocylic complexes ($E^{HOMO}M_{ch} - E^{HOMO}M_n$) and compare them to the difference of energy levels of the corresponding monomacrocyclic complexes. This difference decreases in the order of **7Cu$_n$Ni$_{ch}$** > **7Cu$_n$Cu$_{ch}$** > **7Ni$_n$Cu$_{ch}$**, proving significant interactions in molecules with centers of the most differing donor abilities.

Conclusions

We introduce a new type of dinuclear face-to-face complex composed of tetraazamacrocyclic units of very similar structure but with different charges. All four complexes involving all four possible combinations of the copper and nickel coordinating sites, neutral and charged, were synthesized and characterized.

The molecules studied form three-dimensional (3D) lattices utilizing numerous weak intermolecular interactions. Bismacrocyclic cations are packed in such a way as to optimize interactions between the macrocyclic fragments from neighboring molecules. This leads to stacks of charged and neutral subunits in alternate arrangements. The inter- and intramolecular interactions between the macrocyclic building blocks are exhibited by the decreased metal-to-metal distances of ca. 4.5−4.7 Å. At such intramolecular distances, interactions can be readily detected by electrochemical techniques.

The presence of a charged macrocyclic complex in the bismacrocyclic molecule decreases the electron-donor abilities of the other center. This resembles the common behavior of a redox center in the presence of an electron-withdrawing substituent in the molecule—the donation of the electron to the electrode becomes more difficult. The donor neutral and charged components in the bismacrocylic molecule interact with each other affecting their redox behavior compared to those of isolated metal centers. The energy levels of monomacrocyclic complexes are different from those in the bismacrocyclic compounds with significant enhancement of intramolecular interactions in molecules composed of centers most different in their donor properties to the electrode.

(20) Thelakkat, M.; Schmidt, H.-W. *Adv. Mater.* **1998**, *10*, 219–223.
(21) Bauer, P.; Wietasch, H.; Linder, S. M.; Thelakkat, M. *Chem. Mater.* **2007**, *19*, 88–94.

Experimental Section

Materials and Synthesis. Spectroscopic Measurements. The NMR spectra were obtained with Bruker DRX500 Avance, Varian Mercury 400, and Varian Gemini 2000BB spectrometers. Signals are reported in ppm relative to the residual solvent signal. IR spectra (paraffin oil mulls) were recorded with a Perkin-Elmer Spectrum 2000 FT-IR spectrometer. UV/vis absorption spectra were recorded with a Perkin-Elmer Lambda 25 spectrometer. Mass spectra were measured with a Mariner Perseptive Biosystem and a 4000 QTRAP (ElectroSpray) or Waters GCT Premier Micromass (Field Desorption) mass spectrometers.

Materials. The solvents and reagents used in these studies were reagent grade or better. Acetonitrile and dichloromethane were dried over P_2O_5 and distilled under argon. Macrocyclic ligand $\mathbf{L_1}$,[22] neutral complexes 6,13-bis(carbometoxy)-1,4,8,11-tetraazacyclotetradeca-4,6,11,13-tetraenato(2-)-$\kappa^4N^{1,4,8,11}$ copper(II) and nickel(II) ($\mathbf{1Cu_n}$ and $\mathbf{1Ni_n}$)[15] as well as charged complexes 6,13-bis(methoxymethylidene)-1,4,8,11-tetraazacyclotetradeca-4,7,11,14-tetraene-$\kappa^4N^{1,4,8,11}$copper(II) and nickel(II) bis(heksafluorophosphates) ($\mathbf{6Cu_{ch}}$ and $\mathbf{6Ni_{ch}}$)[23] were synthesized according to the previously published procedures.

Synthesis. 6,13-Bis[carbo(5-hydroxypentoxy)]-1,4,8,11-tetraazacyclotetradeca-4,6,11,13-tetraenato(2-)-$\kappa^4N^{1,4,8,11}$ nickel(II) ($\mathbf{2Ni_n}$). Sodium metal (0.30 g, 13.7 mmol) was dissolved in pentane-1,5-diol (85 mL), then complex $\mathbf{1Ni_n}$ (1.71 g, 4.7 mmol) was added, and the mixture was stirred for 24 h at 100 °C. The resulting dark-orange solution was poured into distilled water (250 mL) and left overnight in the refrigerator. The orange precipitate was filtered off and washed with water and a small amount of methanol. The crude product was dissolved in a dichloromethane/methanol 1:1 mixture (70 mL) and crystallized upon slow evaporation of the solvents. The orange crystals were dried in vacuo over P_2O_5 . Yield: 1.67 g (70%). Mp 172−174 °C; elemental analysis calcd for $C_{22}H_{34}N_4O_6Ni$ (509.22): C, 51.9; H, 6.7; N, 11.0%; Found: C, 51.7; H, 6.9; N, 10.8%; FD-MS (CH_2Cl_2, *m*/*z*): 508.4 ($[C_{22}H_{34}N_4O_6Ni]^+$); IR (nujol, cm^{-1}): 3465 m, 1650s, 1591s, 1536s, 1278s, 1133s; ^1H NMR ($CDCl_3$, 200 MHz, ppm): 1.81−1.56 m (12H, CH_2- β,γ to $-CO_2$, and CH_2- β to −OH), 3.46 s (8H, N−CH_2−CH_2−N), 3.74 t (4H, J = 6.0 Hz, CH_2- α to −OH), 7.88 s (4H, ring N−CH); ^{13}C NMR ($CDCl_3$, 50 MHz, ppm): 22.4($-CH_2-$ β to $-CO_2$), 28.9 ($-CH_2-$ γ to $-CO_2$), 32.4 ($-CH_2-$ β to −OH), 58.7 (N−CH_2−CH_2−N), 62.8 (CH_2- α to $-CO_2$), 63.3 (CH_2- α to −OH), 99.4 (ring *meso* −C═), 154.9 (ring N═CH), 167.1 (O−C═O).

6,13-Bis[carbo(5-hydroxypentoxy)]-1,4,8,11-tetraazacyclotetradeca-4,6,11,13-tetraenato(2-)-$\kappa^4N^{1,4,8,11}$ copper(II) ($\mathbf{2Cu_n}$). Complex was obtained from $\mathbf{1Cu_n}$, following the same procedure as above. Yield: 66%. Mp 140−142 °C; elemental analysis calcd for $C_{22}H_{34}N_4O_6Cu\cdot H_2O$ (531.80): C, 49.6; H, 6.8; N, 10.5%; Found: C, 49.7; H, 6.5; N, 10.5%; ESI-MS (CH_2Cl_2, *m*/*z*): 514.2 ($[C_{22}H_{34}N_4O_6Cu + H^+]^+$), 536.2 ($[C_{22}H_{34}N_4O_6Cu + Na^+]^+$); IR (nujol, cm^{-1}): 3461 m, 1652 m, 1587 s, 1463s, 1270s, 1129s.

6,13-Bis[carbo(3-metanosulfonyloxypentoxy)]-1,4,8,11-tetraazacyclotetradeca-4,6,11,13-tetraenato(2-)-$\kappa^4N^{1,4,8,11}$nickel(II) ($\mathbf{3Ni_n}$). Methanesulfonyl chloride (0.8 mL, 10 mmol) was added to solution of complex $\mathbf{2Ni_n}$ (1.67 g, 3.3 mmol) and triethylamine (1.5 mL, 10 mmol) in dichloromethane (120 mL). The reaction mixture was stirred at room temperature for 24 h. The solution was then concentrated and diluted with ethanol (100 mL), and an orange product was precipitated upon slow evaporation of the solvents. The solid was filtered off, washed with ethanol, and dried in vacuo (2.0 g, 90%). Mp 170−172 °C; elemental analysis calcd for $C_{24}H_{38}N_4O_{10}S_2Ni$ (665.41): C, 43.3; H, 5.8; N, 8.4%; Found: C, 43.3; H, 5.7; N, 8.4%; FD-MS (CH_2Cl_2, *m*/*z*): 664.4 ($[C_{24}H_{38}N_4O_{10}S_2Ni]^+$); IR (nujol, cm^{-1}): 1666 s, 1603 s, 1540 m, 1348 s, 1272 s, 1175 s, 1130 s; ^1H NMR ($CDCl_3$, 200 MHz, ppm): 1.60 m (4H, CH_2- γ to $-CO_2$), 1.82 m (8H, CH_2- β to −OH and CH_2- β to $-CO_2$), 3.08 s (6H, SO_2-CH_3), 3.47 s (8H, N−CH_2−CH_2−N), 4.24 t (4H, J = 6.3 Hz, α to $-OSO_2$), 4.32 t (4H, J = 6.3 Hz, CH_2- α to $-CO_2$), 7.87 s (4H, ring N═CH).

6,13-Bis[carbo(3-metanosulfonyloxypentoxy)]-1,4,8,11-tetraazacyclotetradeca-4,6,11,13-tetraenato(2-)-$\kappa^4N^{1,4,8,11}$copper(II) ($\mathbf{3Cu_n}$). $\mathbf{3Cu_n}$ was obtained from $\mathbf{2Cu_n}$ following the same procedure as above. Yield: 77%. Mp 168−170 °C; elemental analysis calcd for $C_{24}H_{38}N_4O_{10}S_2Cu$ (670.26): C, 43.0; H, 5.7; N, 8.4%; Found: C, 43.2; H, 5.7; N, 8.3%; FD-MS (CH_2Cl_2, *m*/*z*): 669.2 ($[C_{24}H_{38}N_4O_{10}S_2Cu]^+$); ESI-MS ($CH_2Cl_2$, *m*/*z*): 670.3 ($[C_{24}H_{38}N_4O_{10}S_2Cu + H^+]^+$), 692.3 ($[C_{24}H_{38}N_4O_{10}S_2Cu + Na^+]^+$); IR (nujol, cm^{-1}): 1678 s, 1605 s, 1550 m, 1351s, 1265 s, 1163 s, 1129s.

6,13-Bis[(5-azidopentoxy)carbonyl]-1,4,8,11-tetraazacyclotetradeca-4,6,11,13-tetraenato(2-)-$\kappa^4N^{1,4,8,11}$copper(II) ($\mathbf{4Cu_n}$). The mixture of sodium azide (3.9 g, 60 mmol) and tetrabutylammonium bromide (0.97 g, 3 mmol) in water (15 mL) was added to the solution of complex $\mathbf{3Cu_n}$ (1.006 g, 1.5 mmol) dissolved in 40 mL dichloromethane. The mixture was vigorously stirred at room temperature. After 48 h an organic layer was separated, washed with water (3 × 50 mL), and dried over Na_2SO_4. The product was purified by chromatography on neutral Al_2O_3 using dichloromethane as an eluent. The first red band was collected, evaporated to dryness, and crystallized from CH_2Cl_2/MeOH (1:1) solution upon slow evaporation of solvents. Yield 0.685 g (82%). Elemental analysis calcd for $C_{22}H_{32}N_{10}O_4Cu\cdot 1/2CH_3OH$ (580.12): C, 46.6; H, 5.9; N, 24.1%; Found: C, 46.3; H, 5.7; N, 24.0%; FD-MS (CH_2Cl_2, *m*/*z*): 563.2($[C_{22}H_{32}N_{10}O_4Cu]^+$); IR (nujol, cm^{-1}): 2092 m, 1673 m, 1603 s, 1543 m, 1261 s, 1119 m.

6,13-Bis[(5-azidopentoxy)carbonyl]-1,4,8,11-tetraazacyclotetradeca-4,6,11,13-tetraenato(2-)-$\kappa^4N^{1,4,8,11}$ nickel(II) ($\mathbf{4Ni_n}$). $\mathbf{4Ni_n}$ was obtained from $\mathbf{3Ni_n}$ according to the same procedure. Yield 74%. Elemental analysis calcd for $C_{22}H_{32}N_{10}O_4Ni$ (559.25): C, 47.3; H, 5.8; N, 25.0%; Found: C, 47.2; H, 5.8; N, 24.9%; FD-MS (CH_2Cl_2, *m*/*z*): 558.2 ($[C_{22}H_{32}N_{10}O_4Ni]^+$); IR (nujol, cm^{-1}): 2091 m, 1674 m, 1602 m, 1534 w, 1269 m, 1120 w; ^1H NMR ($CDCl_3$, 400 MHz, ppm): 1.48 m (4H, $-CH_2-$ γ to $-CO_2$), 1.66 m (8H, $-CH_2-$ β to $-CO_2$ and $-CH_2-$ β to $-N_3$), 3.29 t (4H, J = 6.6 Hz, CH_2- α to $-N_3$), 3.39 s (8H, N−CH_2−CH_2−N), 4.16 t (4H, J = 6,4 Hz, $-CH_2-$ α to $-CO_2$), 7.81 s (4H, ring −CH═N); ^{13}C NMR ($CDCl_3$, 100 MHz, ppm): 23.4 (CH_2- γ to $-CO_2$), 28.5 and 28.6 (CH_2- β to $-CO_2-$ and $-CH_2-$ β to $-N_3$), 51.3(CH_2- α to $-N_3$), 58.7 (N−CH_2−CH_2−N), 63.0 ($-CH_2-$ α to $-CO_2$), 98.3 (ring *meso* −C═), 154.9 (ring −CH═N), 167.8 (O−C═O).

6,13-Bis[(5-ammoniumpentoxy)carbonyl]-1,4,8,11-tetraazacyclotetradeca-4,6,11,13-tetraenato(2-)-$\kappa^4N^{1,4,8,11}$copper(II) bis(hexafluorophosphate) ($\mathbf{5Cu_n}$). Triphenylphosphine was added (0.284 g, 1.08 mmol) to a solution of $\mathbf{4Cu_n}$ (0.25 g, 0.44 mmol) in 25 mL of dichloromethane. The resulting mixture was stirred at room temperature for 72 h and then 50 mL of methanol and 20 mL of water were added with continuous stirring. After 1 h the mixture was diluted with another 50 mL of water containing 1 mL of acetic acid. The mixture was washed with dichloromethane (3 × 75 mL), and the crystalline product was precipitated after addition of an excess of ammonium hexafluorophosphate (2 g). The product was filtered off and dried in vacuo over phosphorus pentoxide. Yield: 0.313 g (87%). Elemental analysis calcd for $C_{22}H_{38}N_6O_4CuP_2F_{12}$ (804.05): C, 32.9; H, 4.8; N, 10.5%; Found: C, 33.4; H, 4.7; N, 10.4%; ESI-MS (CH_2Cl_2, *m*/*z*): 256.6 ($[C_{22}H_{38}N_6O_4Cu]^{2+}$); IR (nujol, cm^{-1}): 3302 w, 3273 w, 1648 m, 1596 s, 1557 w, 1274 s, 1137 m.

(22) Takamura, S.; Yoshimiya, T.; Kameyama, S.; Nishida, A.; Yamamoto, H.; Noguchi, M. *Synthesis* **2000**, *5*, 637–639.
(23) Korybut-Daszkiewicz, B.; Wieckowska, A.; Bilewicz, R.; Domagała, S.; Woźniak, K. *J. Am. Chem. Soc.* **2001**, *123*, 9356–9366.

6,13-Bis[(5-ammoniumpentoxy)carbonyl]-1,4,8,11-tetraazacyclotetradeca-4,6,11,13-tetraenato(2-)-$\kappa^4N^{1,4,8,11}$ nickel(II) bis(hexafluorophosphate) ($\mathbf{5Ni_n}$). $\mathbf{5Ni_n}$ was obtained from $\mathbf{4Ni_n}$ according to the same procedure. Yield: 89%. Elemental analysis calcd for $C_{22}H_{38}N_6O_4NiP_2F_{12}$ (798.16): C, 33.1; H, 4.8; N, 10.5%; Found: C, 33.1; H, 4.8; N, 10.4%; ESI-MS (CH_3CN, m/z): 254.1-($[C_{22}H_{38}N_6O_4Ni]^{2+}$), 507.2 ($[C_{22}H_{38}N_6O_4Ni - H^+]^+$); IR (nujol, cm^{-1}): 3304 m, 3273 m, 1647 m, 1597 s, 1548 m, 1282 s, 1142 m; ^1H NMR (CD_3CN, 200 MHz, ppm): 1.40 m (4H, CH_2- γ to $-CO_2$), 1.65 m (4H, $-CH_2-$ β to $-CO_2$), 1.65 m (4H, $-CH_2-$ β to $-NH_3$), 2.93 t (4H, J = 7.5 Hz, CH_2- α to $-NH_3$), 3.37 s (8H, $N-CH_2-CH_2-N$), 4.08 t (4H, J = 6.3 Hz, $-CH_2-$ α to $-CO_2$), 6.1bs (6H, $-NH_3$) 7.78 s (4H, ring $-CH=N$); ^{13}C NMR (CD_3CN, 50 MHz, ppm): 23.4 ($-CH_2-$ γ to $-CO_2$), 27.5 ($-CH_2-$ β to $-CO_2$), 29.1 (CH_2- β to $-NH_3$), 41.1 (CH_2- α to $-NH_3$), 59.5 ($N-CH_2-CH_2-N$), 63.3 (CH_2- α to $-CO_2$), 98.3 (ring *meso* $-C=$), 155.7 (ring $-CH=N$), 168.2 ($O-C=O$).

3,19-Dioxa-2,20-dioxo-1^3,1^6,1^{10},1^{13},9,11^3,11^6,11^{10},11^{13},13-decaaza-1-[(1,8)-cyclotetradeca-1,6,8,13-tetraenata(2-)-$\kappa^4N^{3,6,10,13}$-nickel(II)]-11-[(1,8)-cyklotetradeca-2,6,9,13-tetraena-$\kappa^4N^{3,6,10,13}$-nickel(II)]-eikozacyclophane-10,11-diene bis(hexafluorophosphate) ($\mathbf{7Ni_nNi_{ch}}$). Separately prepared solutions of complexes $\mathbf{5Ni_n}$ (0.096 g, 0.12 mmol in 20 mL CH_3CN) and $\mathbf{6Ni_{ch}}$ (0.075 g, 0.12 mmol in 20 mL CH_3CN) were added at a rate of 10 mL h^{-1} by means of a syringe pump to 20 mL of stirred acetonitrile containing *N*-ethyldiisopropylamine (0.041 mL, 0.24 mmol). After the addition was complete, the mixture was stirred at room temperature for 1 h. The crude product was collected by an addition of 0.5 g ammonium hexafluorophosphate and 0.5 mL HCl in 100 mL of water. The precipitated solid was filtered off and washed with water (3 × 50 mL). The product was dissolved in an acetonotrile−water (1:1) mixture, applied to a silica gel 60 silanized (Merck, 0.063−0.200 mm) column, and eluted using a CH_3CN-H_2O (10:9) solution containing 2% of NH_4PF_6. The major orange fraction was collected, and the product crystallized upon slow evaporation of solvent. Orange crystals were filtered off, washed with water, and dried in vacuo. Yield: 0.075 g (58%). Elemental analysis calcd for $C_{34}H_{48}N_{10}O_4Ni_2P_2F_{12}\cdot H_2O$ (1086.14): C, 37.6; H, 4.6; N, 12.9%; Found: C, 37.5; H, 4.9; N, 13.1%; ESI-MS (CH_3CN, m/z): 388.1 ($[C_{34}H_{48}N_{10}O_4Ni_2]^{2+}$), 775.3 ($[C_{34}H_{48}N_{10}O_4Ni_2 - H^+]^+$), 921.2 ($[C_{34}H_{48}N_{10}O_4Ni_2 + PF_6^-]^+$); IR (nujol, cm^{-1}): 3360 m, 3204 m, 1660 m, 1614 s, 1528 m, 1272 s, 1127 s; ^1H NMR (CD_3CN, 500 MHz, ppm): 1.46 m (4H, CH_2- γ to $-CO_2$), 1.62 m (4H, $-CH_2-$ β to $-CO_2$), 1.67 m (4H, $-CH_2-$ β to $-NH$), 3.47 s (8H, $N-CH_2-CH_2-N$), 3.56 t (4H, J = 5.4 Hz, CH_2- α to $-NH$), 3.64 s (8H, $N-CH_2-CH_2-N$), 4.12 t (4H, J = 4,9 Hz, CH_2- α to $-CO_2$), 7.47 d (2H, J =10.5 Hz, $HC=N$) 7.64 d (2H, J = 7,9 Hz, $C=CH-N$), 7.69 s (4H, ring $N-CH$), 7.94 d (2H, J = 9.6 Hz, $HC=N$), 8.04 s (2H, $-NH$); ^{13}C NMR (D, 50 MHz, ppm): 22.7 ($-CH_2-$ γ to $-CO_2$), 28.7 ($-CH_2-$ β to $-CO_2$), 28.8 ($-CH_2-$ β to $-NH$), 51.2 (CH_2- α to $-NH$), 59.5 ($N-CH_2-CH_2-N$),), 59.7 ($N-CH_2-CH_2-N$), 59.8 ($N-CH_2-CH_2-N$), 60.4 ($N-CH_2-CH_2-N$), 60.6 ($N-CH_2-CH_2-N$), 62.9 (CH_2- α to $-CO_2$), 96.7 (*n*-ring *meso* $-C=$), 99.2 (ch-ring *meso* $-C=$), 103.9 (ch-ring *meso* $-C=$), 155.3 ($HC=N$), 155.7 (ring $N=CH$), 160.8 ($HC=N$), 164.2 ($C=CH-N$), 168.0 ($O-C=O$); UV−vis [CH_3CN, λ in nm, (ε)]: 227 (45 037), 287 (53 103), 313 (53 623), 378 (36 262), 483 (975).

3,19-Dioxa-2,20-dioxo-1^3,1^6,1^{10},1^{13},9,11^3,11^6,11^{10},11^{13},13-decaaza-1-[(1,8)-cyclotetradeca-1,6,8,13-tetraenata(2-)-$\kappa^4N^{3,6,10,13}$-copper(II)]-11-[(1,8)-cyklotetradeca-2,6,9,13-tetraena-$\kappa^4N^{3,6,10,13}$-copper(II)]-eikozacyclophane-10,11-diene bis(hexafluorophosphate) ($\mathbf{7Cu_nCu_{ch}}$). $\mathbf{7Cu_nCu_{ch}}$ was obtained from complexes $\mathbf{5Cu_n}$ and $\mathbf{6Cu_{ch}}$ according to the same procedure. Yield: 25%. Elemental analysis calcd for $C_{34}H_{48}N_{10}O_4Cu_2P_2F_{12}\cdot H_2O\cdot CH_3CN$ (1136.90): C, 38.0; H, 4.7; N, 13.6%; Found: C, 38.0; H, 4.7; N, 13.4%; ESI-MS (CH_3CN, m/z): 393.1 ($[C_{34}H_{48}N_{10}O_4Cu_2]^{2+}$); IR (nujol, cm^{-1}): 3363 m, 3229 w, 1661 m, 1617s, 1536 m, 1266 s, 1130 s; UV−vis [CH_3CN, λ in nm, (ε)]: 205 (41 020), 284 (103 232), 311 (41 864), 323 (46 915), 349 (35 304), 522 (323).

3,19-Dioxa-2,20-dioxo-1^3,1^6,1^{10},1^{13},9,11^3,11^6,11^{10},11^{13},13-decaaza-1-[(1,8)-cyclotetradeca-1,6,8,13-tetraenata(2-)-$\kappa^4N^{3,6,10,13}$-copper(II)]-11-[(1,8)-cyklotetradeca-2,6,9,13-tetraena-$\kappa^4N^{3,6,10,13}$-nickel(II)]-eikozacyclophane-10,11-diene bis(hexafluorophosphate) ($\mathbf{7Cu_nNi_{ch}}$). $\mathbf{7Cu_nNi_{ch}}$ was obtained from complexes $\mathbf{5Cu_n}$ and $\mathbf{6Ni_{ch}}$ according to the same procedure. Yield: 32%. Elemental analysis calcd for $C_{34}H_{48}N_{10}O_4CuNiP_2F_{12}\cdot H_2O\cdot CH_3CN$ (1132.04): C, 38.2; H, 4.7; N, 13.6%; Found: C, 38.2; H, 4.7; N, 13.6%; ESI-MS (CH_3CN, m/z): 390.9 ($[C_{34}H_{48}N_{10}O_4CuNi]^{2+}$), 780.3 ($[C_{34}H_{48}N_{10}O_4CuNi - H^+]^+$); IR (nujol, cm^{-1}): 3362 w, 3228 w, 1659 s, 1615 s, 1538 m, 1270 s, 1131 m; UV−vis [CH_3CN, λ in nm, (ε)]: 284 (94 037), 309 (29 425), 323 (30 209), 378 (24 361), 427 (1297).

3,19-Dioxa-2,20-dioxo-1^3,1^6,1^{10},1^{13},9,11^3,11^6,11^{10},11^{13},13-decaaza-1-[(1,8)-cyclotetradeca-1,6,8,13-tetraenata(2-)-$\kappa^4N^{3,6,10,13}$-nickel(II)]-11-[(1,8)-cyklotetradeca-2,6,9,13-tetraena-$\kappa^4N^{3,6,10,13}$-copper(II)]-eikozacyclophane-10,11-diene bis(hexafluorophosphate) ($\mathbf{7Ni_nCu_{ch}}$). $\mathbf{7Ni_nCu_{ch}}$ was obtained from complexes $\mathbf{5Ni_n}$ and $\mathbf{6Cu_{ch}}$ according to the same procedure. Yield: 40%. Elemental analysis calcd for $C_{34}H_{48}N_{10}O_4CuNiP_2F_{12}$ (1072.98): C, 38.1; H, 4.5; N, 13.1%; Found: C, 38.1; H, 4.4; N, 12.8%; ESI-MS (CH_3CN, m/z): 390.9 ($[C_{34}H_{38}N_{10}O_4CuNi]^{2+}$), 780.3 ($[C_{34}H_{38}N_{10}O_4CuNi - H^+]^+$); IR (nujol, cm^{-1}): 3362 w, 3238 w, 1661 m, 1617 s, 1529 m, 1273 s, 1132 m; UV−vis [CH_3CN, λ in nm, (ε)]: 206 (30 540), 226 (34 732), 287 (52 232), 312 (52 394), 351 (26 382), 436 (2099), 514 (485).

6,13-Bis(butylaminomethylidene)-1,4,8,11-tetraazacyclotetradeca-4,7,11,14-tetraene-$\kappa^4N^{1,4,8,11}$ copper(II) bis(hexafluorophosphate) ($\mathbf{8Cu_{ch}}$). Butylamine (0.058 mL; 0.59 mmol) was added to a solution of complex **6Cu** (0.15 g, 0.24 mmol) in 25 mL of CH_3CN. This solution was stirred at room temperature for 24 h. After the reaction was completed, 0.5 g of ammonium hexafluorophosphate and 0.5 mL of HCl in 100 mL of water was added. Slow evaporation of acetonitrile resulted in crystallization of deep red plates of $\mathbf{8Cu_{ch}}$. The product was filtered off and dried in vacuo over phosphorus pentoxide. Yield: 0.152 g (79%). Elemental analysis calcd for $C_{20}H_{34}N_6CuP_2F_{12}$ (712.00): C, 33.7; H, 4.8; N, 11.8%; Found: C, 33.4; H, 4.9; N, 11.8%; ESI-MS (CH_3CN, m/z): 210.5 ($[C_{20}H_{34}N_6Cu]^{2+}$), 420.2 ($[C_{20}H_{34}N_6Cu - H^+]^+$), 566.2 ($[C_{20}H_{34}N_6Cu + (PF6)^-]^+$); IR (nujol, cm^{-1}): 3385 w, 1618 s, 1568 w. UV−vis [CH_3CN, λ in nm, (ε)]: 349 (46 706), 509 (262).

6,13-Bis(butylaminomethylidene)-1,4,8,11-tetraazacyclotetradeca-4,7,11,14-tetraene-$\kappa^4N^{1,4,8,11}$nickel(II) bis(hexafluorophosphate) ($\mathbf{8Ni_{ch}}$). $\mathbf{8Ni_{ch}}$ was synthesized from nickel(II) complex **6Ni** following the same procedure. Yield: 73% of orange crystals. Elemental analysis calcd for $C_{20}H_{34}N_6NiP_2F_{12}$ (707.15): C, 34.0; H, 4.8; N, 11.9%; Found: C, 34.0; H, 5.0; N, 11.8%; ESI-MS (CH_3CN, m/z): 208.1 ($[C_{20}H_{34}N_6Ni]^{2+}$), 415.2 ($[C_{20}H_{34}N_6Ni - H^+]^+$), 561.20 ($[C_{20}H_{34}N_6Ni + (PF_6)^-]^+$; IR (nujol, cm^{-1}): 3387 w, 1634 s, 1561 w; ^1H NMR (CD_3CN, 500 MHz, ppm) 0.93 t (6H, J = 7.2 Hz, $-CH_2-$ δ to $-NH$), 1.36 se (4H, J = 7.3 Hz, $-CH_2-$ γ to $-NH$), 1.62 q (4H, J =7.1 Hz, $-CH_2-$ β to $-NH$), 3.42−3.58 m (8H, $N-CH_2-CH_2-N$), 3.42−3.58 m (4H, CH_2- α to $-NH$), 7.48 s (2H, ring $HC=N$) 7.59 d (2H, J = 16.0 Hz, $C=CH-N$), 7.96 s (2H, ring $HC=N$), 8.08 d (2H, J = 16.0 Hz, $-NH$); ^{13}C NMR (CD_3CN, 50 MHz, ppm): 13.7 ($-CH_2-$ δ to $-NH$), 20.0 ($-CH_2-$ γ to $-NH$), 32.3 ($-CH_2-$ β to $-NH$), 51.4 (CH_2- α to $-NH$), 59.3 ($N-CH_2-CH_2-N$),), 59.5 ($N-CH_2-CH_2-N$), 60.2 ($N-CH_2-CH_2-N$), 60.4 ($N-CH_2-CH_2-N$), 104.0 (*meso* $-C=$), 155.0 ($HC=N$), 160.6 ($HC=N$), 163.8 ($C=CH-N$); UV−vis [CH_3CN, λ in nm, (ε)]: 280 (32 537), 378 (32 205), 473 (1046).

Voltammetry. All electrochemical experiments were done in a three-electrode arrangement with a silver/silver chloride (Ag/AgCl) as the reference, a platinum foil as the counter, and a glassy carbon electrode (GCE, BAS, 3 mm diameter) as the working electrode. The reference electrode was separated from the working solution by an electrolytic bridge filled with a 0.1 M

Table 4. Crystal Data and Summary of Intensity Data Collection and Structure Refinement

compound	$7Ni_nNi_{ch}$	$7Cu_nCu_{ch}$	$7Ni_nCu_{ch}$	$7Cu_nNi_{ch}$
formula	$C_{34}H_{48}N_{10}O_4Ni_2P_2F_{12}\cdot CH_3CN$	$C_{34}H_{48}N_{10}O_4Cu_2P_2F_{12}\cdot H_2O\cdot CH_3CN$	$C_{34}H_{48}N_{10}O_4CuNiP_2F_{12}\cdot H_2O\cdot CH_3CN$	$C_{34}H_{48}N_{10}O_4CuNiP_2F_{12}\cdot H_2O\cdot CH_3CN$
formula weight	1109.2	1134.90	1130.07	1130.07
crystal system	monoclinic	monoclinic	monoclinic	monoclinic
space group	$P2_1/n$	$P2_1/n$	$P2_1/n$	$P2_1/n$
cell constants: a (Å)	7.8962(15)	7.8040(4)	7.862(7)	7.8366(5)
b (Å)	26.681(6)	26.7195(12)	26.82(2)	26.6336(17)
c (Å)	21.615(4)	22.4128(11)	22.446(18)	22.5131(14)
α (deg)	90	90	90	90
β (deg)	90.860(14)	93.805(3)	93.80(2)	94.024(4)
γ (deg)	90	90	90	90
V (Å^3)	4553.4(15)	4663.2(4)	4723(7)	4687.3(5)
molecules/unit cell	4	4	4	4
ρ_{calcd} (g·cm^{-3})	1.618	1.617	1.589	1.601
temp (K)	150.0	150.0	150.0	150.0
abs coeff (mm^{-1})	2.604	2.691	2.597	2.616
cryst size (mm)	0.37 × 0.09 × 0.07	0.40 × 0.20 × 0.10	0.20 × 0.16 × 0.06	0.45 × 0.15 × 0.10
max 2-ϑ (deg)	133.2	133.2	130.16	130.22
index ranges	$-9 \le h \le 8$ $-30 \le k \le 31$ $-24 \le l \le 25$	$-9 \le h \le 8$ $-30 \le k \le 31$ $-26 \le l \le 26$	$-8 \le h \le 9$ $-31 \le k \le 31$ $-22 \le l \le 26$	$-9 \le h \le 8$ $-31 \le k \le 31$ $-25 \le l \le 26$
no. of reflcns collcd	30 408	46 579	28 344	35 245
no. of indpt reflcns	8047	8065	7826	7827
no. of obsd reflcns[a]	3716	5999	3232	5721
refinement method	full matrix on F^2	full matrix on F^2	full matrix on F^2	full matrix on F^2
data/restrain/params	8047/0/643	8065/0/614	7826/0/614	7827/0/615
gof on F^2	0.931	1.048	1.051	1.025
$R1$ indices [$I > 2\sigma(I)$]	0.0681	0.0686	0.0891	0.0781
$wR2$ indices (all data)[b]	0.1998	0.2074	0.2716	0.2166
weight params a, b	0.0933, 0.0000	0.0822, 3.0846	0.1006, 0.0000	0.1018, 16.8875
largest diff peak and hole (e·Å^{-3})	0.56 and −0.42	1.245 and −0.619	0.670 and −0.543	1.12 and −0.71

[a] $|F_o| > 4\sigma(|F_o|)$. [b] $\omega = 1/[\sigma^2(F_o^2) + (0.0532P)^2 + 0.00P]$, where $P = (F_o^2 + 2F_c^2)/3$.

TBAHFP/AN solution. The reference electrode potential was calibrated by using a ferrocene electrode process in the same TBAHFP/AN solution ($E'_{Fc} = 0.425$ V). The acetonitrile (AN) containing 0.1 M tetrabutylammonium hexafluorphosphate (TBAHFP) was used as the supporting electrolyte solution. Argon was used to deaerate the solution, and an argon blanket was maintained over the solution during the experiments. Linear scan and differential pulse voltammetry were performed using the CHI 750B potentiostat (CH Instrument, Austin, TX). All experiments were carried out at 25 °C. The GC electrode was polished mechanically with 1.0, 0.3, and 0.05 μm alumina powder on a Buehler polishing cloth to a mirror-like surface. Finally, it was rinsed thoroughly with acetonitrile and sonificated in pure acetonitrile.

X-ray Crystallography. The X-ray diffraction measurements have been carried out on Bruker-X8 APEX diffractometer with a CCD detector, using graphite-monochromated CuKα radiation. Data were collected at 150 K temperature using ω-2θ scan techniques. The crystals were cooled by a stream of nitrogen. Data reduction was carried out with the BRUKER software. Data were corrected for absorption effects using the face-indexed numerical method (SADABS). The structures were solved by the direct methods using SHELXS86 or SHELXS97[24] and refined by full-matrix methods using the least-squares instructions of SHELXL97.[25] The refinement process was based on F^2 for all reflections. Anisotropic displacement parameters were applied for all non-hydrogen atoms. All of hydrogen atoms were located in idealized averaged geometrical positions, allowed to ride at the heavy atoms, and rotated around C−O and C−C bonds.

Crystallographic data (see Table 4), excluding structural factors, for the structures reported in this paper have been deposited with the Cambridge Crystallographic Data Center and allocated the deposition numbers: CCDC 751 747, 751 748, 751 749, and 751 750 for $7Cu_nCu_{ch}$, $7Cu_nNi_{ch}$, $7Ni_nCu_{ch}$, and $7Ni_nNi_{ch}$, respectively. Copies of the data can be obtained free of charge on application to CCDC, 12 Union Road, Cambridge CB2 1EW, United Kingdom (E-mail: deposit@ccdc.cam.ac.uk).

Acknowledgment. This work was financially supported by Ministry of Science and Higher Education, Project N204 074 32/2022. The X-ray measurements were carried out by Organic Crystallochemistry Research Group, under supervision of Prof. Z. Urbańczyk-Lipkowska at the Institute of Organic Chemistry of Polish Academy of Sciences.

Supporting Information Available: SHELXL data. This material is available free of charge via the Internet at http://pubs.acs.org.

(24) Sheldrick, G. M. *Acta Crystallogr.* **1990**, *A 46*, 467.
(25) Sheldrick, G. M. *SHELXL-97: Program for the Refinement of Crystal Structures*; University of Göttingen: Göttingen, Germany, 1998.